

INVESTIGATION OF IMPACT PERFORMANCE OF CYLINDER CORRUGATED SANDWICH STRUCTURES WITH DIFFERENT GEOMETRIC CONFIGURATIONS

Ilyas BOZKURT 

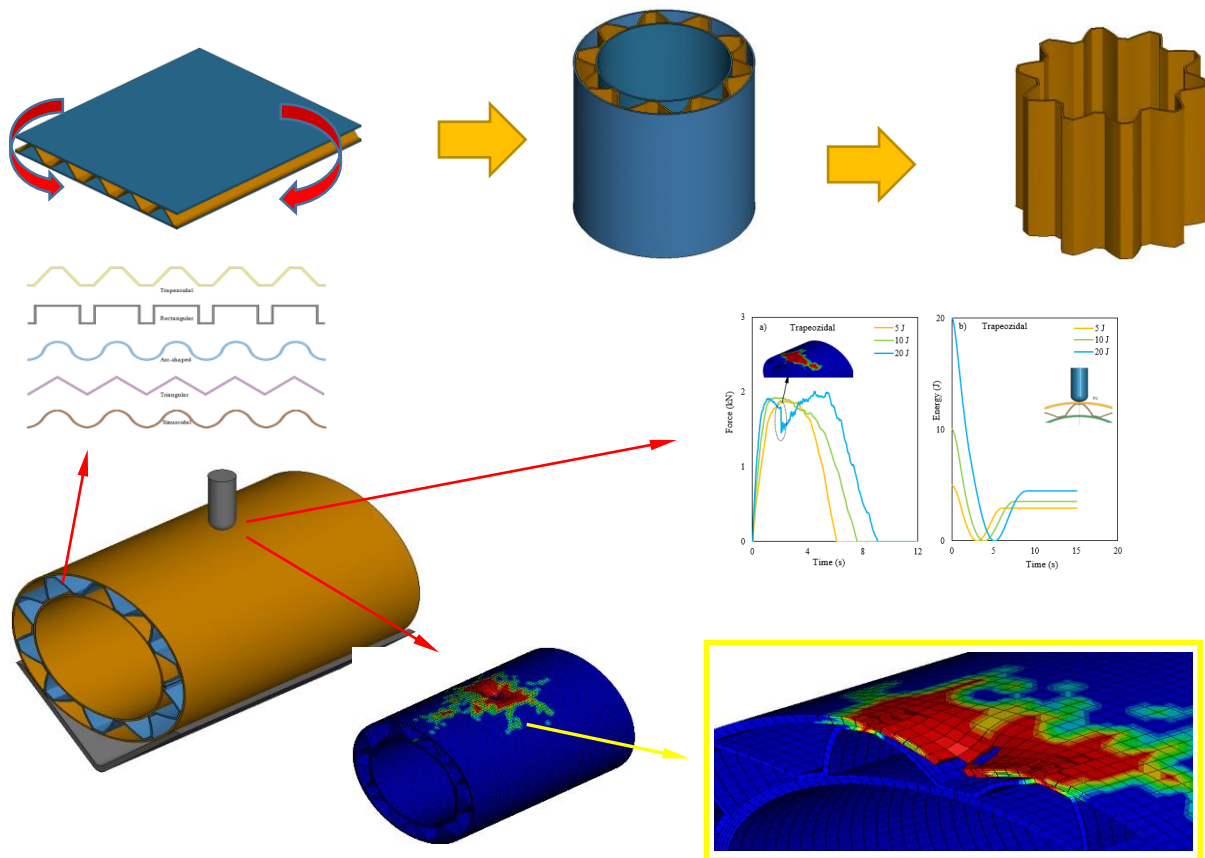
Mus Alparslan University, Architecture and Engineering Faculty, Mechanical Engineering Department, Mus,
TÜRKİYE

i.bozkurt@alparslan.edu.tr

Highlights

- Impact performances of cylindrical sandwich structures with five different core structures are investigated in this study.
- In the study, *progressive damage analysis* is performed based on *Hashin damage criterion* in *LS DYNA* finite element program for low velocity impact simulations.
- The effects of core shape and impact point on Peak contact force, Absorbed energy efficiency, Maximum displacement and deformation are compared.

Graphical Abstract



Flowchart of the proposed method



INVESTIGATION OF IMPACT PERFORMANCE OF CYLINDER CORRUGATED SANDWICH STRUCTURES WITH DIFFERENT GEOMETRIC CONFIGURATIONS

Ilyas BOZKURT 

Mus Alparslan University, Architecture and Engineering Faculty, Mechanical Engineering Department, Mus,
TÜRKİYE
i.bozkurt@alparslan.edu.tr

(Received: 30.07.2024; Accepted in Revised Form: 18.10.2024)

ABSTRACT: The aim of this study is to numerically investigate and compare the impact performance of CFRP composite cylinder sandwich structures with five different geometric configurations. The impact performances and damage types of composite cylinder structures for different core configurations were determined. The impact analyses were performed in *LS DYNA* finite element program using *MAT-54* material model with *Progressive damage analysis* based on the combination of *Hashin damage criterion*, *Cohesive zone model* and *Bilinear traction-separation law*. Among the five different specimens in the study, the highest peak force (PF) value of 1.88 kN was obtained at impact point P2 of the Trapezoidal sandwich structure. The lowest value was obtained at P1 impact point in Triangular sandwich structure with 0.62 kN. The highest and lowest energy absorption efficiency occurred in the Triangular structure, 78% and 38% respectively. The PF value at P2 point is higher than P1. The effect of core support on PF is very important. Since point P1 is not supported by the core, it is determined that the deformation is larger than P2.

Keywords: Sandwich Cylinder Composite, Impact Test, Progressive Damage Analysis, Finite Element Method, Cohesive Zone Model (CZM)

1. INTRODUCTION

Composite materials are used in many sectors, especially in the defense industry, due to their high strength-to-weight ratio and excellent energy absorption capacity against impacts [1]. Sandwich composite structures stand out especially in parts and components where energy absorption is required. Sandwich structures are structures consisting of surfaces such as carbon or glass composites and cores with different shapes and different materials (lattice structures, prismatic structures, honeycomb) [2]. Due to the superior properties of sandwich composite structures, they can be used in many different areas and components and can be exposed to very different loading conditions. Damage to the composite structure may occur as a result of loading during service or unexpected impacts. Especially in the aviation industry and civil aircraft, effects such as bird strikes or turbulence can cause these damages. While these damages are sometimes visible, sometimes they can occur unnoticed in the structure. These invisible damages can grow during service with the effect of fatigue and stress intensity and can cause major disasters. Therefore, it is extremely important for human life to determine how these structures, which help people to travel collectively, such as airplanes and large passenger ships with a high percentage of composite use, will react in the event of impact and to determine the maximum strength limits.

The reaction of composite structures to impact is more difficult to predict than that of metal structures. For example, the reaction of an aluminum specimen to impact can be predicted due to the linearity in the material structure. This process is more difficult in composite structures. Because there are many factors that determine the mechanical properties of the composite structure. For example, fiber type, fiber thickness, matrix type, matrix properties, fiber matrix compatibility, etc. can be counted as many factors affecting the mechanical properties of composite structures. Therefore, it is very important to have healthy information about the mechanics of the structure by determining the mechanical performance of composite structures against impacts by experimental or simulation. In order to determine the mechanical

*Corresponding Author: İlyas BOZKURT, i.bozkurt@alparslan.edu.tr

behavior of composite structures, many high-cost special equipment, laboratories and expert human resources are needed. Access to these high-cost test equipment and production-testing require large budgets. Therefore, this financial problem limits many researchers from doing research in this field. With the development of finite element technology, analyses that give very close results to experimental studies can be performed in computer environment. When the boundary conditions used in the experimental environment are applied, results with high accuracy rates are obtained and researchers can perform many analyzes. However, even variations that cannot be made in experimental environments can be easily realized with Finite Element Technology. Researchers who have limited laboratory facilities and have difficulty in finding financial support can analyze very high cost, complex and difficult experiments with high precision with FEM. Many studies investigating the performance of sandwich composite structures under impact loading have been conducted by researchers. Xue et al. [3] investigated the impact performance of carbon/glass fiber hybrid composite facesheets sandwich structure with nomex honeycomb core for different structural dimensions. Tarafdar et al. [4] investigated the axial behavior of a hybrid multicellular aluminum and GFRP sandwich tube subjected to quasi-static compression and low velocity impact. They experimentally and numerically investigated the effects of material permutation and inner tube diameter using the commercial finite element code LS-DYNA. Chen et al. [5] investigated the collapse behavior of sandwich tubes subjected to falling object impact through finite element (FE) numerical simulation. Sensitive parameter studies were performed to evaluate the influence of falling object mass, kinetic energy and burial depth on the dent characteristics. Gemi et al. [6] experimentally investigated the low velocity impact behavior of glass/carbon functionally graded filament wound composite pipes with $\pm 55^\circ$ winding angle. The hybrid composite tubes were graded with a fixed layer configuration of glass-glass/glass-carbon/carbon-glass/carbon-carbon-carbon from the inside to the outside. The functionally graded hybrid pipes were subjected to different internal pressure values and the impact behavior of the hybrid composite pipes was investigated. Korupolu et al. [7] investigated the performance of hierarchical honeycomb core cellular structures under compressive and impact loads. Hierarchical patterns were developed by replacing the apex cells of regular hexagonal honeycombs with circular cells. The local arrangement of the proposed hierarchical cellular structures was improved to withstand higher loads. Yand et al. [8] experimentally and numerically investigated the impact resistance and failure mechanisms of carbon fiber composite axial and circular corrugated sandwich cylindrical panel structures produced by hot press molding method. The effects of relative density, impact energy and impact location on impact performance were investigated. Bozkurt [9] numerically investigated the low-velocity impact behavior of carbon fiber reinforced orthogonal woven fabric composite sandwich structures with five different geometric configurations and four different curve angles. Low-velocity impact simulations were performed in *LS DYNA* finite element program to investigate the effects of core configuration and curve angle on peak contact force, energy absorption efficiency and failure mode. Ayten [10] focused on how a ply fiber fabric can improve the energy absorption and post-damage behavior of composite structures. For this purpose, the post-impact low velocity and compression behaviors of composite materials with thermoplastic matrix were experimentally investigated. Zheng et al. [11] numerically investigated the transverse impact performance of corrugated sandwich cylindrical tubes. The failure modes, impact load and deformation, and energy absorption capacity of sandwich cylindrical tubes were investigated. He et al. [[12], [13]] investigated the impact behavior of X-type sandwiches consisting of a carbon fiber reinforced polymer surface layer and an aluminum alloy core. Bozkurt et al. [14] experimentally and numerically investigated the impact and compression behaviors of sandwich composite structures composed of fully fiber reinforced composites.

In this study, unlike the literature, the impact performances of CFRP composite cylinder sandwich structures with five different cores were numerically analyzed and compared with each other. In the study, impact performances and damage types of composite cylinder structures were determined for different core structures and different impact points. There are many studies in the literature investigating the impact performance of sandwich structures. However, for the first time in this study, impact performance and damage analysis of cylindrical sandwich structures with five different core structures

were performed. Impact analyses were performed in *LS DYNA* finite element program. At the end of the impact, the tensile strengths and energy absorption performances were compared.

2. NUMERICAL STUDY

2.1. Finite Element Model

Low-velocity impact tests are usually applied to determine the behavior of the material under impact load. These tests provide information about the mechanical performance of the material. As a result of low-velocity impact tests, many graphs are obtained that give information about the material strength. In the low-velocity impact test setup, these data are obtained by reading from the tip of the impactor. With the changes in the kinetic energy and velocity of the impactor, displacement graphs are extracted from its position. Equations (1)-(4) are used to obtain the changes in velocity, displacement and energy with respect to the impact timing of the impactor. Data on contact force, displacement and absorbed energy obtained from the tip of the impactor were evaluated.

$$v(t) = v_i + gt - \int_0^t \frac{F(t)}{m} dt \quad (1)$$

Here, t is the time of the first contact of the impactor to the specimen, which is $t = 0$; $v(t)$ is the velocity of the impactor at time t ; v_i is the velocity of the impactor at time $t = 0$; and $F(t)$ is the impact contact force measured at time t .

$$\delta(t) = \delta_i + v_i t + \frac{gt^2}{2} - \int_0^t \left(\int_0^t \frac{F(t)}{m} dt \right) dt \quad (2)$$

δ is the displacement of the impactor at time t , while δ_i is the displacement of the impactor from the reference point at time $t = 0$.

$$E_a(t) = \frac{m(v_i^2 - (v(t))^2)}{2} + mh\delta(t) \quad (3)$$

Here, $E_a(t)$ is the absorbed energy at time t , m is the weight impact, and g is the gravitational acceleration. To evaluate the weight efficiency of the energy absorption of a structure, the specific energy absorption (*SEA*) is generally used.

$$SEA = \frac{E_a}{m} \quad (4)$$

Here, m is the mass of the crash structure. Higher *SEA* values indicate better energy-absorbing efficiency of the structures.

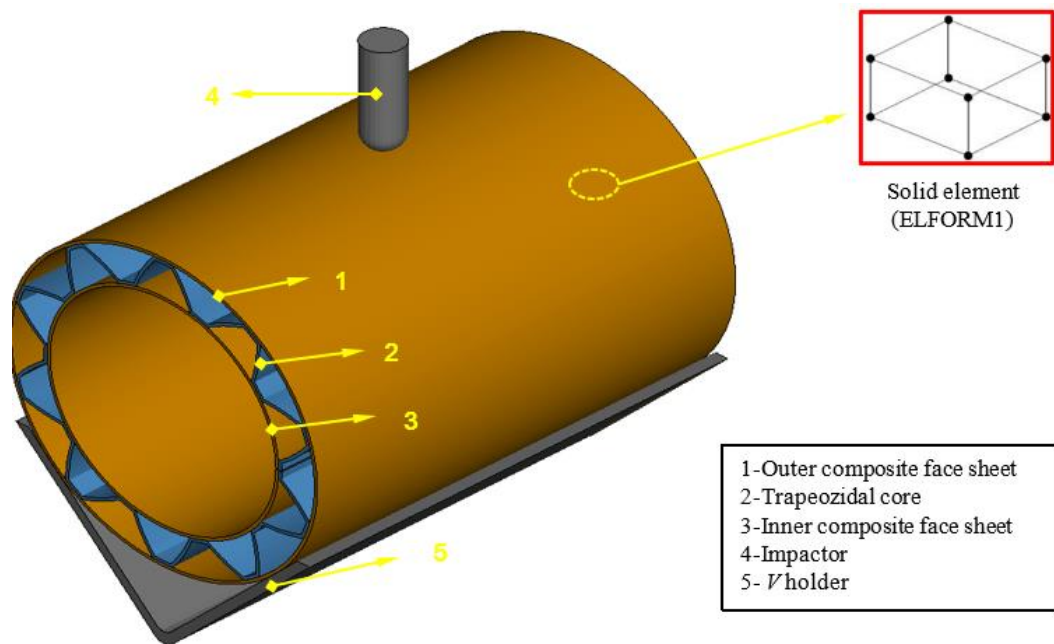


Figure 1. Finite element model of low velocity impact test.

Many finite element programs have been developed to determine the impact behavior of sandwich structures. Among these, *LS-DYNA*, a commercial finite element software program, was preferred due to its large material library, ease of use and the ability to develop complex numerical models [15]. The low velocity impact model of sandwich structures with different core structures is given in Figure 1. For all specimens used in this study, impact tests were performed numerically with a diameter \times length of 100 \times 140 mm. In the study, 8-node brick solid element (*ELFORM1*) was used for all elements. Mesh convergence study was performed and it was seen that the most compatible mesh structure was 2 \times 2 mm considering the processing time and efficiency. The diameter of the hemispherical impactor is 12 mm, the length is 36 mm and the weight is 8.37 kg. When the studies in the literature are examined, the shape of the holder in the impact test of cylinder structures is V-shaped and modeled in a way to prevent the specimen from moving during impact [6], [16]. Experiments were carried out by considering this principle in the experimental studies. The direction of movement of the striker is restricted for x and y directions.

Movement is allowed only for the z direction. V holder is considered completely fixed. That is, its movement is restricted for x , y and z directions. A total of 91551 nodes and 51042 solid elements were used in the modeling. The V holder was modeled with 14768 nodes and 9660 solid elements. The CONTACT_AUTOMATIC_SURFACE_TO_SURFACE contact card was used to model the contact force between the sandwich composite and the impactor and to prevent the specimen from moving between the holders during impact. The static and dynamic friction coefficients were entered as 0.2 and 0.3 respectively [14]. The CONTACT_AUTOMATIC_SINGLE_SURFACE card was used to prevent all elements from interfering with each other due to the impact.

Five different corrugated core structures with different geometric configurations (Trapezoidal, Rectangular, Arc-shaped, Triangular and Sinusoidal) were investigated in the study. Figure 2 shows the shapes of the Trapezoidal, Rectangular, Arc-shaped, Triangular and Sinusoidal core structures used in the study. Core dimensions and specimen shapes of these structures are given in Table 1 and Table 2 respectively. The fabrication process of the specimens is given in Figure 3. Their weights were found by calculating their volumes in FE. Facesheet thickness of all specimens is 2 mm. The cell width and cell heights used in all structures are equal. When their weights are analyzed, it is seen that the largest weight difference is very small, 1.6%. Therefore, by considering their weights equal, the performance of these structures under impact load can be determined and evaluated between the same boundary conditions.

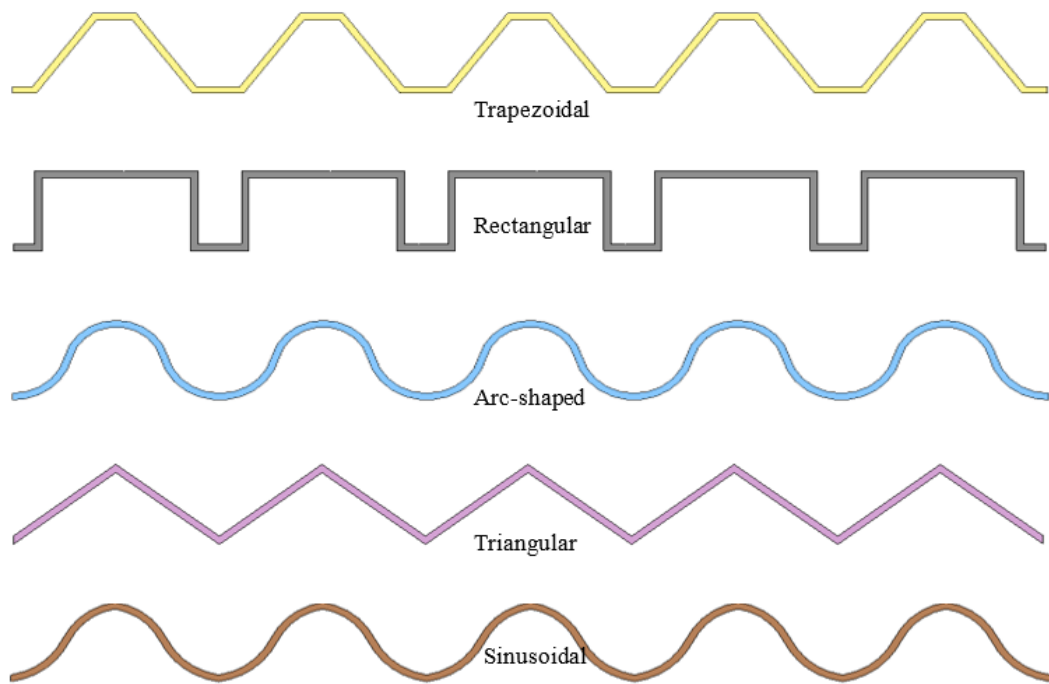


Figure 2. Different corrugated core structures used in the research.

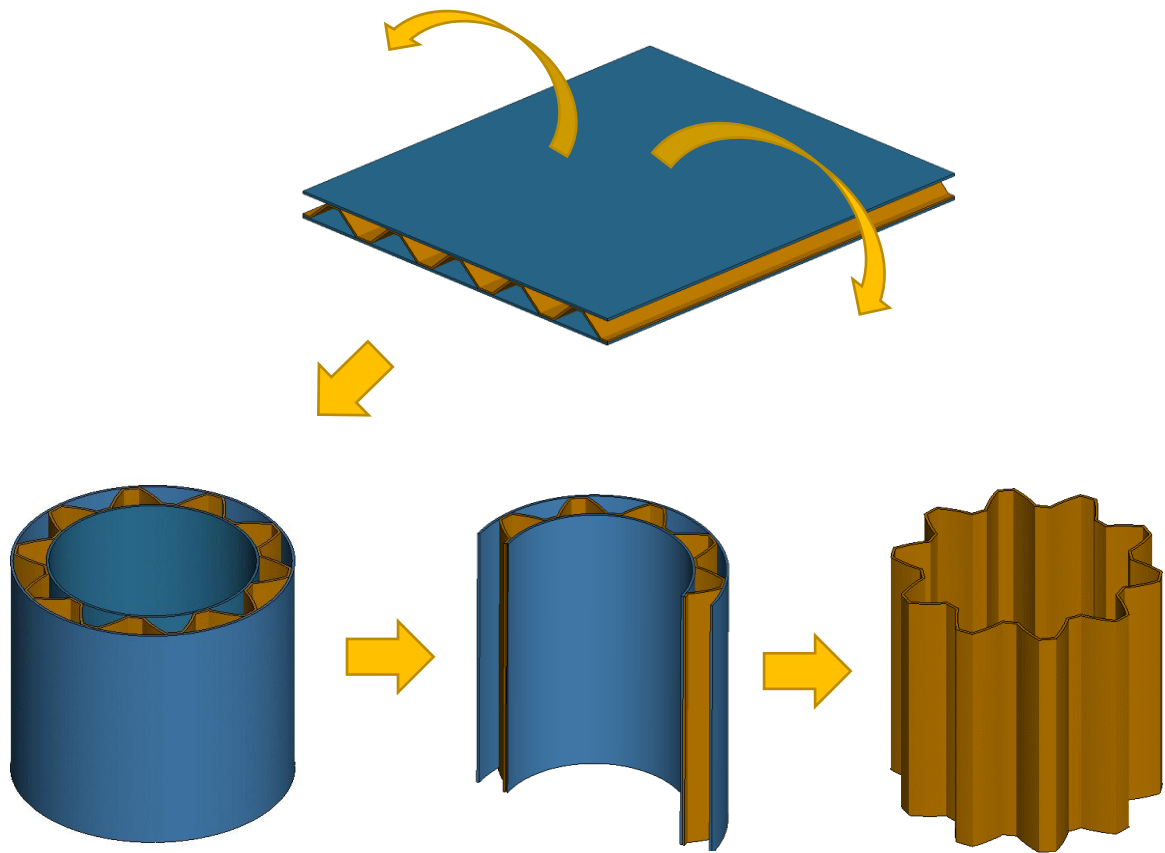


Figure 3. Design process of specimens.

Table 1. Dimensions and masses of corrugated core structures.

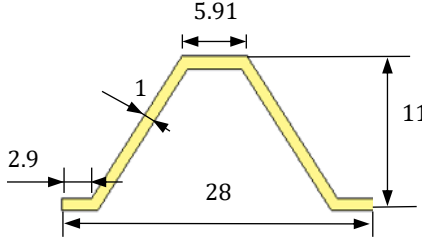
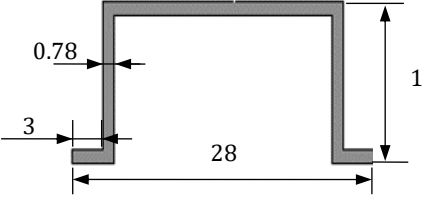
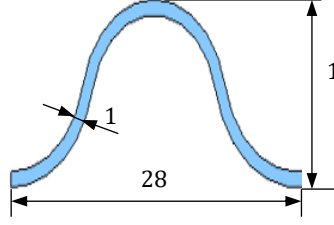
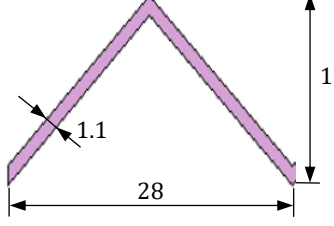
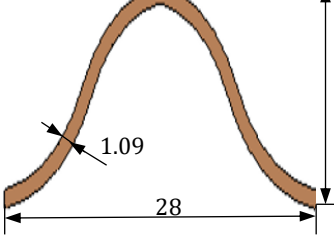
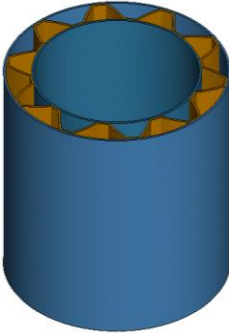
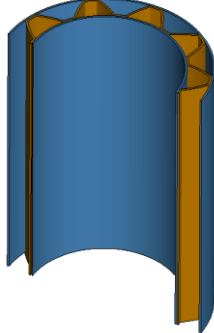
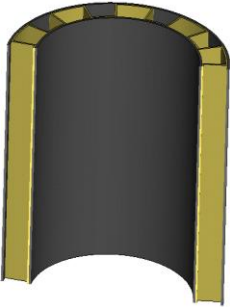
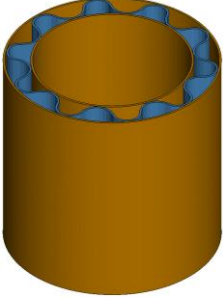
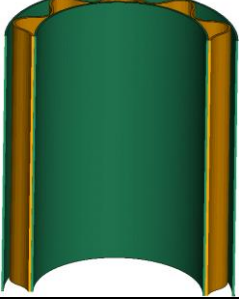
Cell name	Cell Shape	Mass (gr)
Trapezoidal		145.778
Rectangular		145.879
Arc-shaped		144.997
Triangular		146.666
Sinusoidal		147.394

Table 2. Impact specimens.

Specimens	Corrugated core	
Trapezoidal		
Rectangular		
Arc-shaped		
Triangular		
Sinusoidal		

Since the core structures used in the study are corrugated, there are points that support the outer facesheet as well as points that are not supported by the core. Impacts on the specimen surface may come from one of these two points. Therefore, it is necessary to analyze these two different situations and

determine the impact performance. For all specimens, the points not supported by the core are named P1 and the points supported by the core are named P2. These points are given in Figure 4.

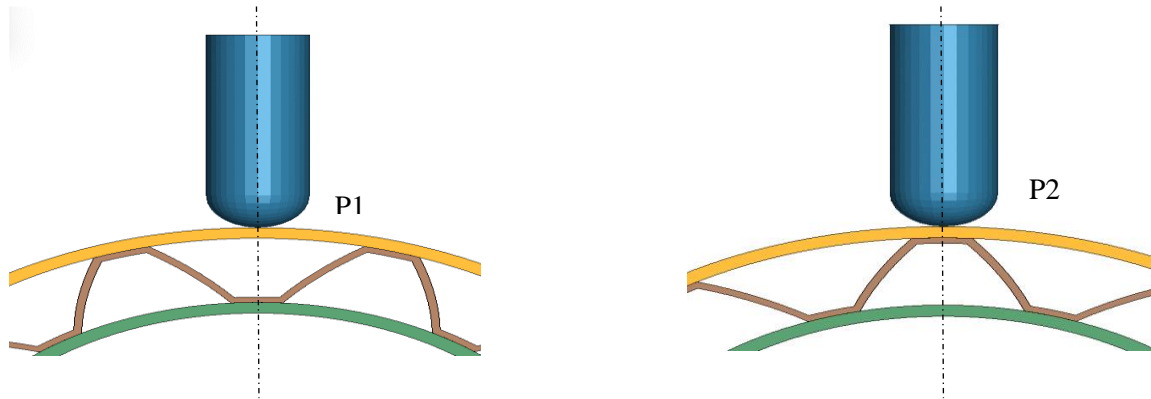


Figure 4. Impact points.

2.2. Modeling of Adhesive Layer

In sandwich composite structures, the core structure in the middle and the upper and lower face sheets must adhere to each other. This adhesion is achieved in the experimental laboratory by applying adhesive materials such as resin or *Araldite-55* to the contact surfaces. Some mechanical rules are adopted during the separation of these two bonded structural elements. In the literature, it is characterized as CZM with a double linear traction-separation law. This law is based on the application of three independent parameters. The traction t_0 between the layers when the force is applied, the separation distance δ_0 when the damage starts and the G_c under this curve. After the impact occurs, the separation between the layers occurs according to this principle (Figure 5)

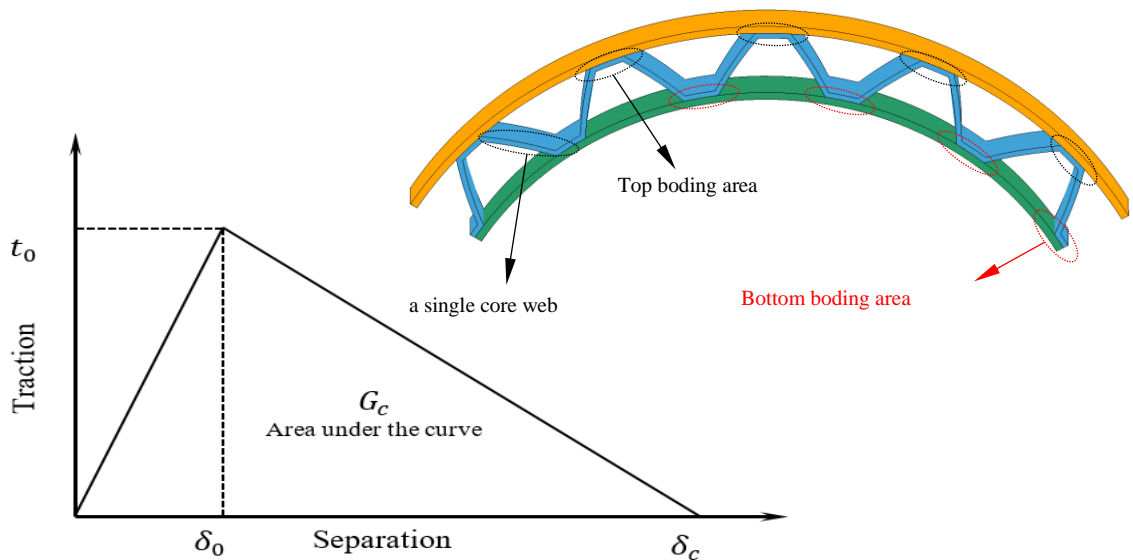


Figure 5. Bilinear traction-separation law

Adhesion here can be achieved in two ways. First, it can be achieved by defining a thin interface material between the top facesheet and the core in the middle. Or it can be achieved by using an adhesion surface that performs the same task. Dogan et al. [17] found this method to be effective instead of using an intermediate material. In this study, The CONTACT_AUTOMATIC SURFACE TO SURFACE

TIEBREAK contact board was used to bond the top and bottom facesheets to the core material in between. Separations occur based on the Bilinear traction-separation law given in Figure 5.

With this contact card, the nodes making contact in the beginning connect with each other according to the following criterion.

$$\left(\frac{|\sigma_n|}{NFLS}\right)^2 + \left(\frac{|\sigma_s|}{SFLS}\right)^2 \geq 1 \quad (5)$$

Here, while σ_n and σ_s are the current normal and shear stresses, *NFLS* and *SFLS* are respectively the interface and shear strength. When the condition of Equation (8) is met, interface node stress is decreased to zero and the connection between the nodes is released. The contact parameters for Araldite 2015, which was used as the adhesive material in this research, are provided in Table 3.

Table 3. Cohesive parameters of delamination between core and face sheets interfaces [14].

Contact Tiebreak Variable	Description	Value	Units
<i>NFLS</i>	Peak traction in normal direction	21.63x109	Pa
<i>SFLS</i>	Peak traction in tangential direction	17.9x109	Pa
<i>PARAM</i>	Exponent of mixed-mode criteria	1	-
<i>ERATEN</i>	Energy release rate for Mode I	430	N/m
<i>ERATES</i>	Energy release rate for Mode II	4700	N/m
<i>CT2CN</i>	Ratio of tangential stiffness to normal stiffness	1	-
<i>CN</i>	Normal stiffness	8080	Pa/m

2.3. Material Models

There are many material models that describe composite materials in the *LS-DYNA* finite element program. The choice of these models varies according to the intended use. *MAT 54* material model was used in this study. In this material model, fiber damage, matrix damage and delamination behavior under impact loading can be determined based on the progressive damage principle. Hashin damage criteria [15] are applied with this material model. A total of 24 parameters are required to introduce the *MAT 54* material model to the program. Details of these parameters are given in Table 4-5.

2.4. MAT_54-55: Enhanced Composite Damage Model

It is the most widely used material model in the analysis of composite structures. In the material model, it is assumed that the material is orthotropic and linear elastic in the absence of any damage. In this model, *MAT 54* damage criterion was proposed by Chang and *MAT 55* damage criterion was proposed by Tsai-Wu. The working logic of this material model and *MAT 22* model is the same but additionally includes the compression damage mode. The Chang-Chang criterion (*MAT 54*) is given below;

Tensile fibre ($\sigma_{11} > 0$).

$$\left(\frac{\sigma_{11}}{s_1}\right)^2 + \bar{\tau} = 1 \quad (6)$$

All moduli and Poisson's ratios are set to zero when the tensile fibre failure criteria are met, that is $E_1 = E_2 = G_{12} = \nu_{12} = \nu_{21} = 0$. All the stresses in the elements are reduced to zero, and the element layer has failed.

Failure mode for compressive fibre ($\sigma_{11} > 0$),

Table 4. Mechanical parameters of the CFRP composite [14].

Symbol	Property	Value	Unit
ρ	Density	1500	kg/m ³
E_a, E_b	Young modulus a and b direction	43.7	GPa
E_c	Young modulus in c direction	14.57	GPa
ν_{ab}	Poisson's ratio in ab plane	0.21	-
ν_{bc}	Poisson's ratio in bc plane	0.21	-
ν_{ca}	Poisson's ratio in ca plane	0.21	-
G_{ab}	Shear modulus in ab plane	14.18	GPa
G_{bc}	Shear modulus in bc plane	14.65	GPa
G_{ca}	Shear modulus in ca plane	14.65	GPa
S_{aT}	Tensile strength a direction	0.589	GPa
S_{aC}	Compressive strength a direction	0.1096	GPa
S_{bT}	Tensile strength b direction	0.589	GPa
S_{bC}	Compressive strength b direction	0.1096	GPa
S_{ab}	Shear strength in ab plane	0.1082	GPa

Table 5. Failure parameters of the CFRP composite.

Symbol	Description	Unit
$DFAILM$	Transverse matrix failure strain experimental	0.0
$DFAILS$	Shear failure strain experimental	0.0
$DFAILT$	Tensile fiber failure strain experimental	0.0
$DFAILC$	Compressive fiber failure strain experimental	0.0
$TFAIL$	Timestep for element deletion computational	0.16
$Alpha$	Shear stress parameter damage dependent	0.0
$Soft$	Strength reduction factor damage dependent	0.7
$FBRT$	Reduction factor for X_t damage dependent	1
$YCFAC$	Reduction factor for X_c damage dependent	3
EFS	Efective failure strain computational	0.90

$$\left(\frac{\sigma_{11}}{S_{12}}\right)^2 = 1 \quad (7)$$

Failure mode for tensile matrix ($\sigma_{11} > 0$),

$$\left(\frac{\sigma_{22}}{S_2}\right)^2 + \bar{\tau} = 1 \quad (8)$$

Failure mode for compressive matrix

$$\left(\frac{\sigma_{22}}{2S_{12}}\right)^2 + \left[\left(\frac{C_2}{2S_{12}}\right) - 1\right] \frac{\sigma_{22}}{C_2} + \bar{\tau} = 1 \quad (9)$$

Where E_1 and E_2 are the longitudinal and transverse elastic moduli, respectively, G_{12} is the shear modulus, ν_{12} and ν_{21} are the in-plane Poisson's ratios.

3. RESULTS AND DISCUSSION

Low-velocity impact tests are usually applied to determine the behavior of the material under impact load. These tests provide information about the mechanical performance of the material. As a result of low-velocity impact tests, many graphs that give information about material strength are obtained. Among these graphs, Contact force-time, Contact force-displacement and energy-time graphs are given in Figure 6. Contact force-time graph shows the change in time when the impactor contacts the specimen. When Peak force (PF) reaches the maximum value of this graph, the contact force decreases and approaches zero. When the force approaches zero, this means that the impactor leaves the surface of the specimen and moves back. This return can be seen in the contact force -displacement graph. The maximum displacement of the impact is shown as PFD.

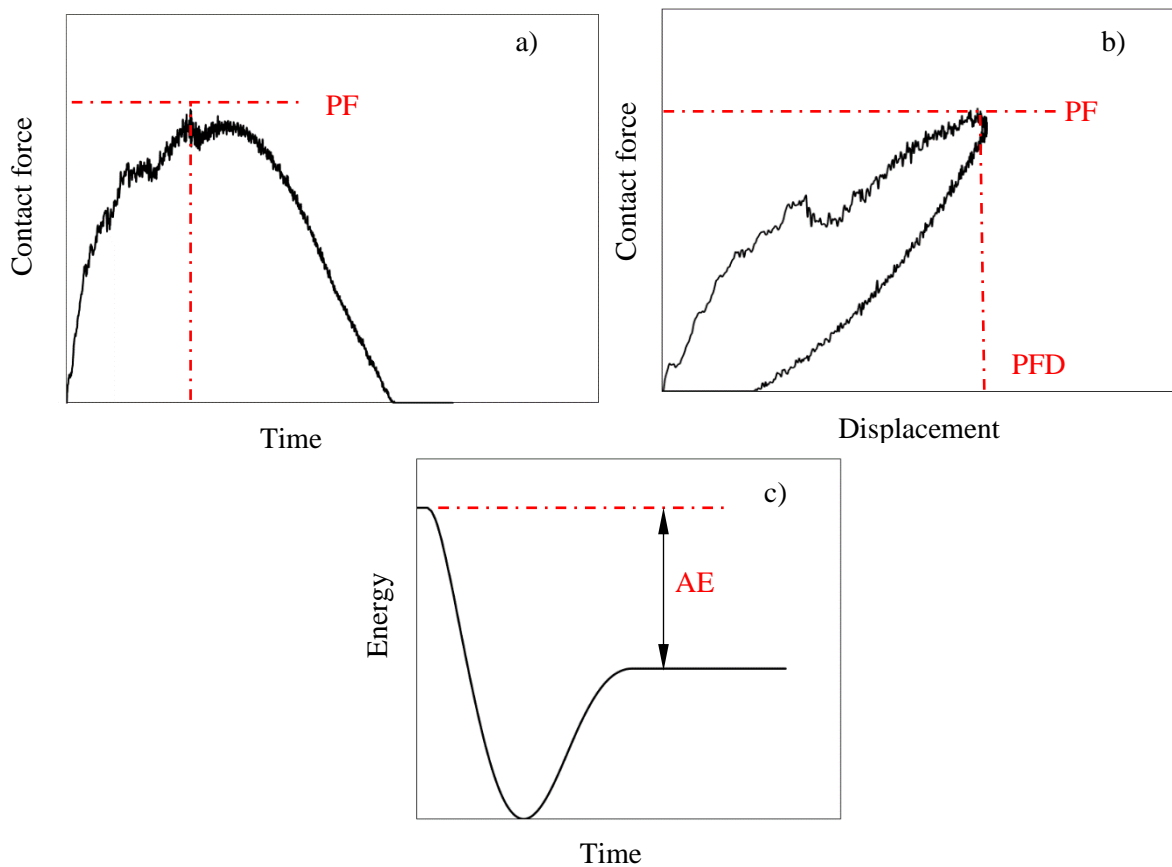


Figure 6. a) Contact force-time, b) Contact force -displacement and c) Energy-time graphs of composite structures under impact load.

The energy-time graph helps us to obtain the absorbed energy (AE) value of the specimen by determining the difference between the initial and final energies of the impactor. In the impact test, different types of impact loading can occur according to the velocity of the impactor. If the impact velocity is less than 10 m/s, it is called low velocity, and if it is between 10 m/s and 50 m/s, it is called medium velocity impact. If the impact speed is between 50 m/s and 1000 m/s, it is called high-speed impact [14].

Contact force-time, absorbed energy-time, contact force-displacement and velocity-time graphs for different impact energies of circular sandwich structure with trapezoidal core are given in Figure 7. In the contact force-time graph in Figure 7a, the force reaches its maximum point due to the contact of the impactor with the specimen surface and then returns to zero point with energy dissipation. Here it is understood that the impactor bounces back on the specimen surface and breaks contact with the specimen. In other words, it has shown elastic properties here and the rebounding effect has occurred. As the force

reaches its peak, oscillations are observed in the graphs for all three different impact energies. Since damage occurs in the specimen layers with the impact, very small force drops are experienced. Therefore, oscillations occur in the graph [8]. For impact energies of 5, 10 and 20 J, the peak contact forces were determined as 1.16, 1.40 and 1.89 kN, respectively. As the impact energy increased, the contact force increased in parallel. In the energy-time graph in Figure 7b, while the initial impact energies were 5, 10 and 20 J, the energy values at the end of the test were determined as 1.48, 0.52 and 1.12 J, respectively. Here, when the remaining energy value is subtracted from the initial energy, the energy value absorbed by the specimen is obtained. The amount of absorbed energy is divided by the initial energy to obtain the absorbed energy value in %. This is called energy absorption efficiency. Accordingly, energy absorption efficiency values were determined as 70% , 94.5% and 94.4% respectively. Energy absorption efficiency reaches a certain level and then enters a decline phase. In the contact force-displacement graph in Figure 7c, it is seen that the contact force and displacement value increase with the impact energy. For impact energies of 5, 10 and 20 J, the maximum displacements were determined as 3.88, 6.30 and 13.71 mm, respectively. As the impact energy increased, the displacement value also increased [17]. In the velocity-time graph in Figure 7d, the velocity of the impactor was determined as 1.090, 1.545 and 3.443 m/s for impact energies of 5, 10 and 20 J, respectively. When the graph is carefully examined, it is seen that the velocity of the impactor passes from the positive state to the negative field. Here, it is understood that the impactor first moves from +z to -z and then returns back again. When the contact is interrupted, it continues at the initial speed.

In Figure 8, the mechanical performance of the same core structure, i.e. the sandwich structure with Trapezoidal core, is examined in case of impact at point P2. In the contact force-time graph of Figure 8a, the force value reached the peak point for 5 and 10 J and then returned to zero without fluctuation. When the energy of the impactor was 20 j, the force value reached the peak point and then there was a sharp drop in the force value. This is due to the damage to the top layer. The deformation is shown on the graph. In addition, since point P2 is supported by the core, there is not much fluctuation. However, when the graph of the analysis for the P1 point is examined, it is seen that there are large fluctuations and oscillatory movements even at 5 J impact. Here, the important effect of the core structure on PF is understood. In the energy-time graph of Figure 8b, some of the energy of the impactor is absorbed. However, compared to P1, this ratio is lower. In the contact force-displacement graph in Figure 8c, the displacement value increases as the impact energy increases. Also, the return point of the force is seen on the graph. As the impact energy increases, the return point of the force value also increases.

Figure 9 shows the peak force and energy absorption efficiency values of sandwich structures with five different core configurations under different impact energies. When the graph is analyzed for 5 J in Figure 9a, the PF value at P2 points is higher than P1. This is because it is supported by the core structure. The highest peak force value with 1.88 kN was obtained at the P2 impact point in the trapezoidal sandwich structure. The lowest value was obtained at the P1 impact point in the Triangular sandwich structure with 0.62 kN. When the energy absorption efficiencies were analyzed, it was determined that the absorption efficiency for the P1 impact point was higher than the P2 point. In other words, it absorbed the impact energy coming to the P1 point more and sent the impactor back with less energy. The highest energy absorption efficiency was Triangular with 0.78 and the lowest was Triangular with 0.38. In Figure 9b, it is seen that the PF value increases for 10 J and the maximum peak force value is in the Rectangular structure with 2.05. The highest energy absorption efficiency occurred in the Triangular structure with 0.94. In general, the energy absorption efficiency value increased as the impact energy increased [9].

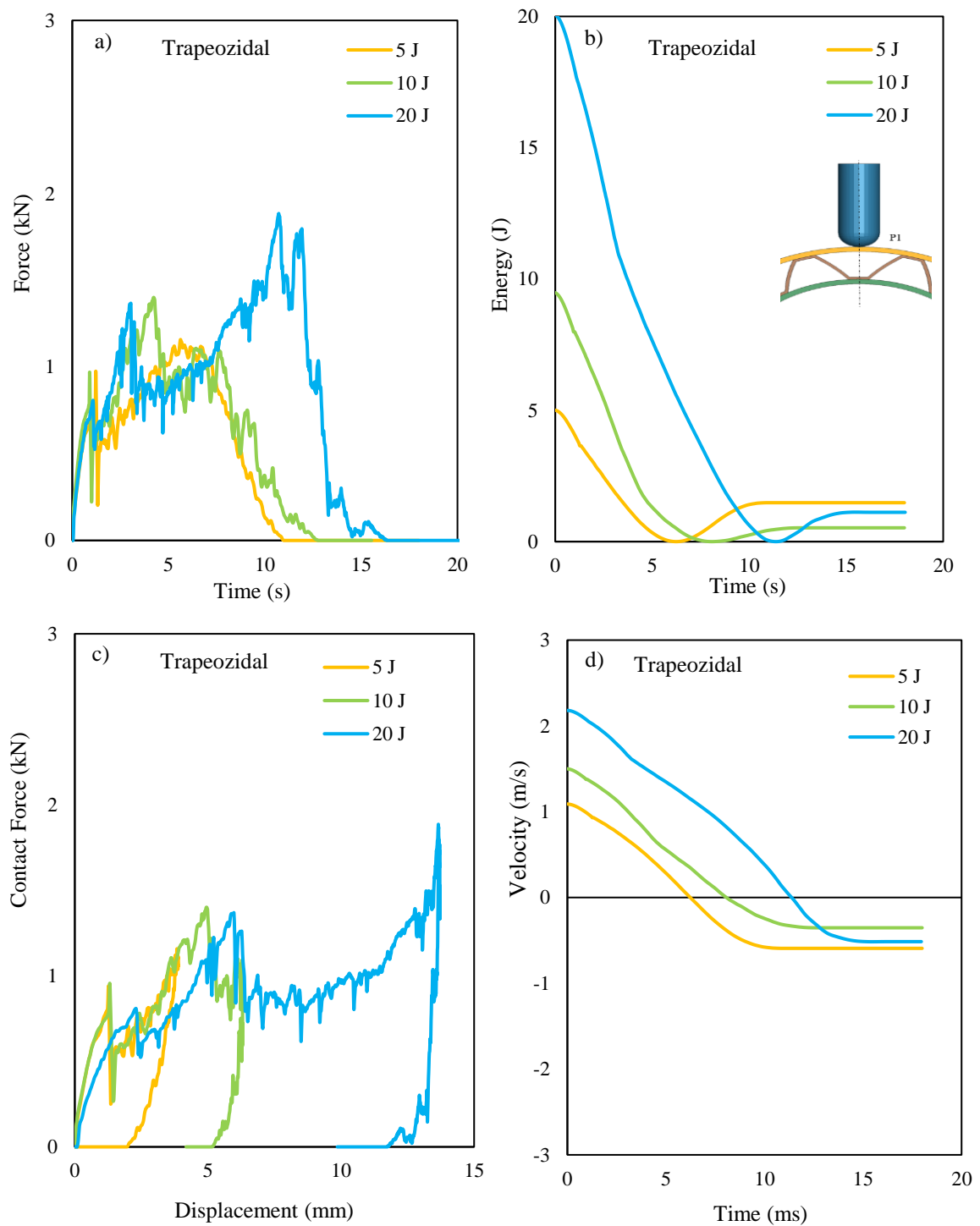


Figure 7. Variation of a) Contact force-Time, b) Energy-Time, c) Contact force-Displacement and d) Velocity-Time graphs with impact energy (P1 Impact point).

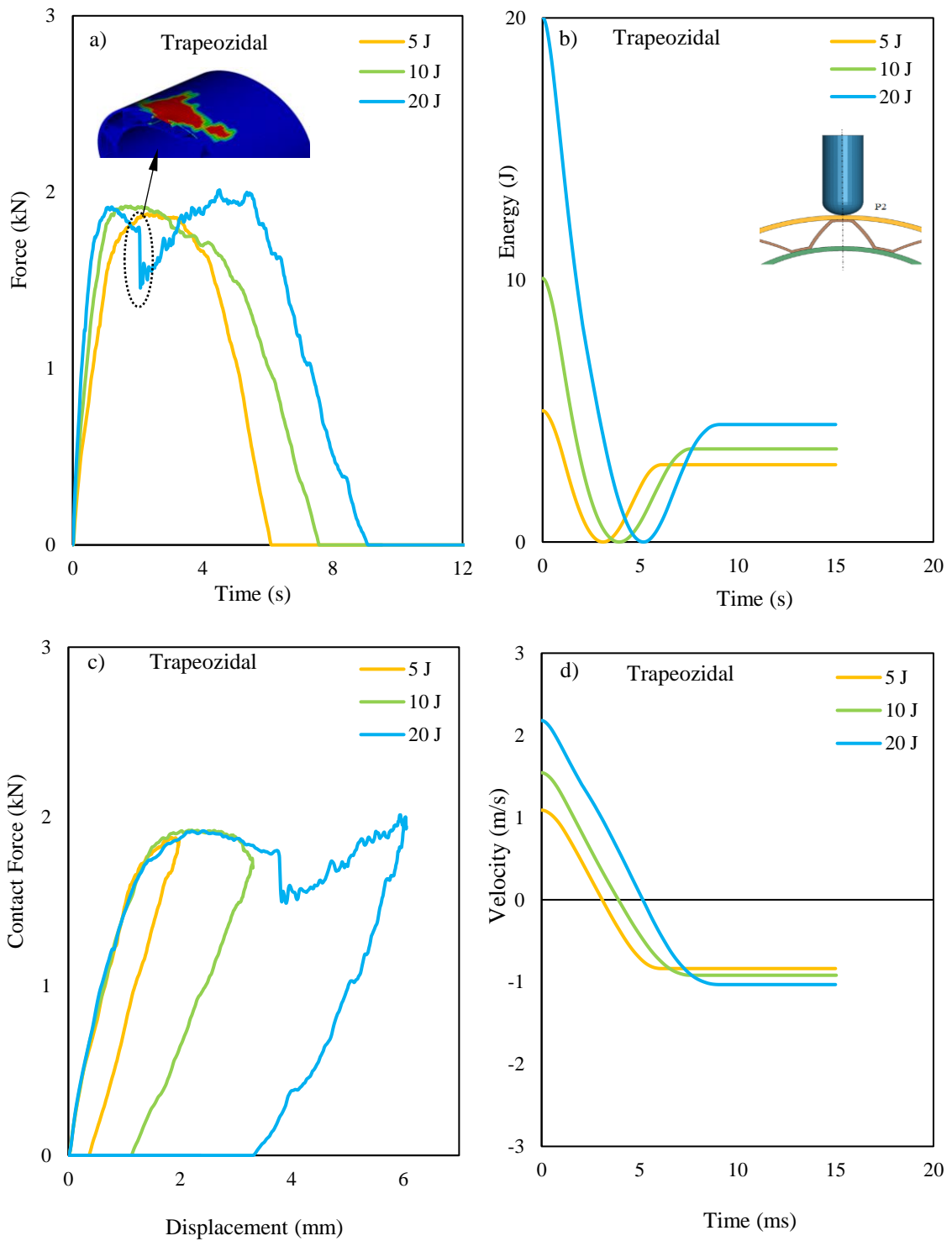


Figure 8. Variation of a) Contact force-Time, b) Energy-Time, c) Contact force-Displacement and d) Velocity-Time graphs with impact energy (P2 Impact point).

When the graph for 20 J is analyzed in Figure 9c, the PF value at P1 points is higher than the PF values obtained at some P2 points. This is because the structure has reached its maximum strength point. Even if the impact energy increases after a point, the contact force value will no longer increase [8]. In triangular the PF value at point P1 exceeded that at point P2. In sinusoidal structure, P2 PF value exceeded P1 value.

The maximum PF occurred in Rectangular structure with 2.45 kN and the minimum occurred in Sinusoidal structure with 1.22 kN. Energy absorption efficiency was highest in Sinusoidal structure with 0.95 and lowest in Sinusoidal structure with 0.69.

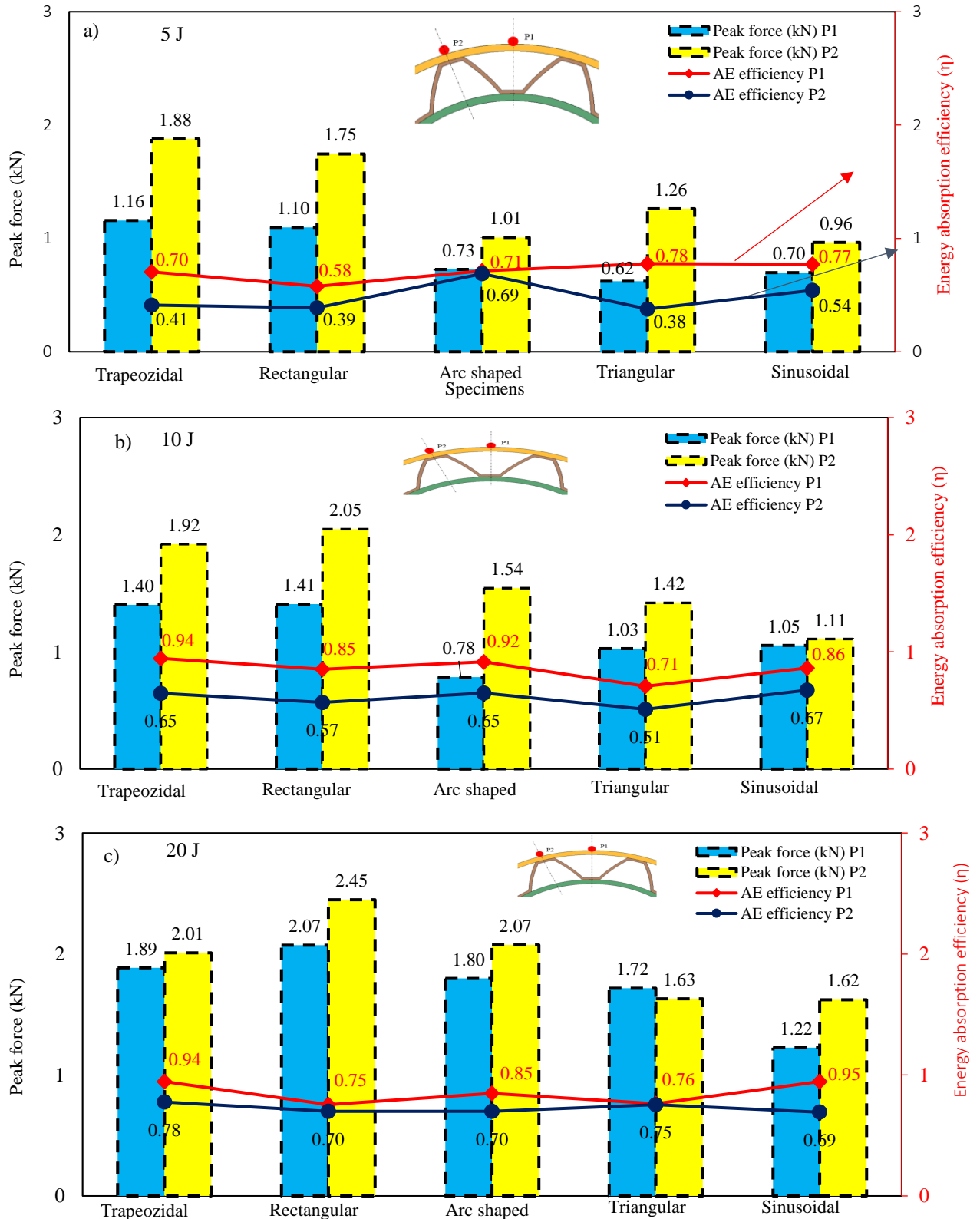


Figure 9. Effect of impact point variation on contact force and absorbed energy efficiency variation.

One of the most important conveniences offered by the finite element method is the ability to see the deformations at the intended point during the impact simulation [18]. In low-velocity impact tests performed under laboratory conditions, it is not possible to see the deformation progression because the test time is very short. Thanks to the developing camera technology, it is possible to watch with high-resolution cameras that record slow motion. However, the high cost of these devices limits access to them. Therefore, with FEM, damage progression can be easily seen without any cost [11]. In Figure 10, the contact force-time graph of the sandwich structure with Trapezoidal core is given as a result of 10 J impact on P1 and P2 points. In both graphs, material deformations at the same contact moments are given. In this way, material deformations at certain points can be compared.

When the graph is analyzed, the waves and oscillations resulting from the impact on the note P1 are much higher than P2. This means that too much breakage and damage occurred. While the first damage at P1 occurred at $t=0.039$ ms, it occurred at P2 at $t=0.24$ ms. It can be seen how the damage progresses as time progresses. At point P1, the damage is higher because there is no core support. At P2, with core support, the oscillations in the graph are very small and the damage is less.

When composite structures are subjected to impact, they react with composite damage types such as matrix cracking, fiber fracture or delamination in order to absorb this energy. In the impacted structure, the matrix structure absorbs the incoming energy first. If the intensity of the impact is high, it causes delamination between the layers. Fibers are the most robust component of the structure [19]. If fracture occurs in the fibers, the damage process is completed and the structure is damaged [20]. Here the performance of the composite structure depends on many factors. There are many factors such as matrix type, matrix structure holding the fibers together, matrix fiber compatibility, fiber orientation. In fact, these many factors are one of the reasons why composite structures are widely researched and investigated with a large number of experimental and finite element methods. All researchers are working in this field to design a cost-effective and optimum structure.

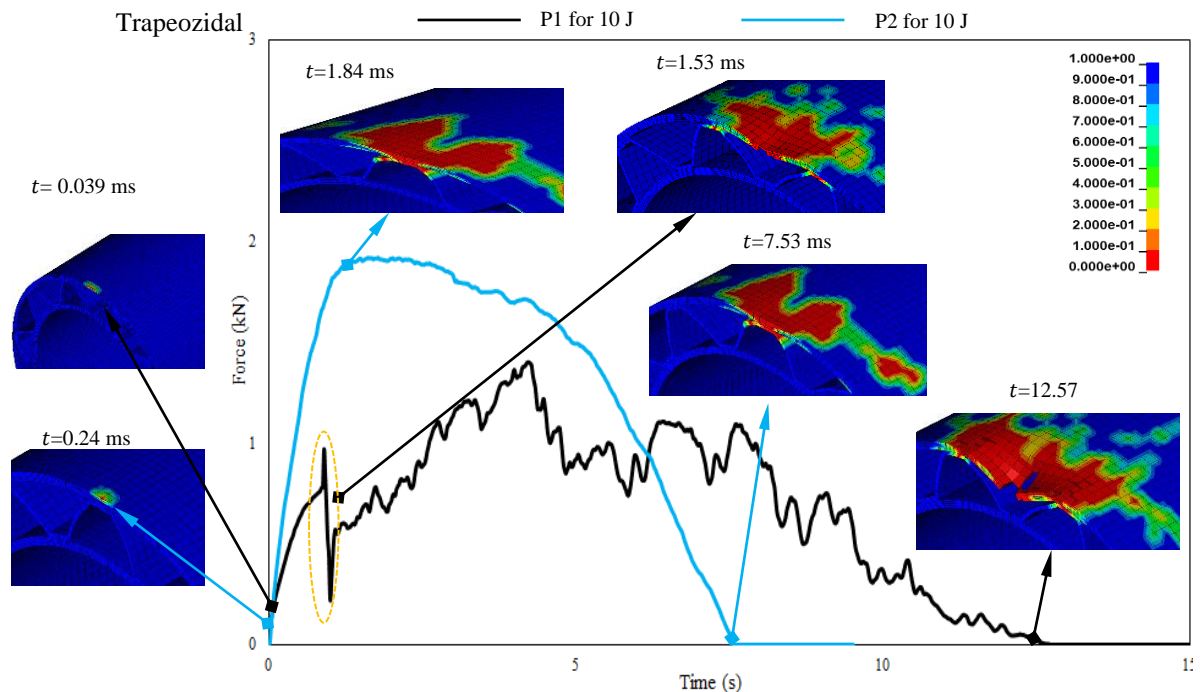
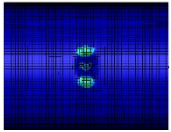
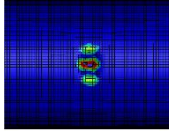
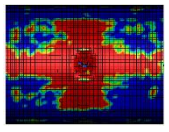
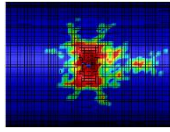
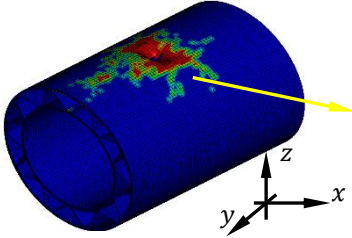
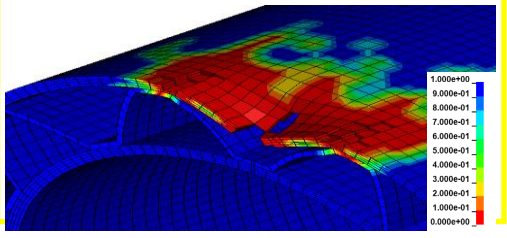
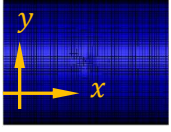
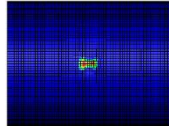
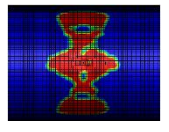
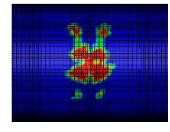
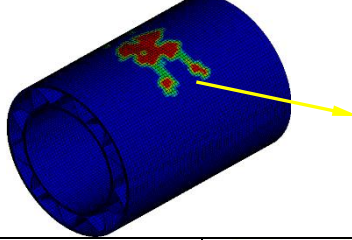
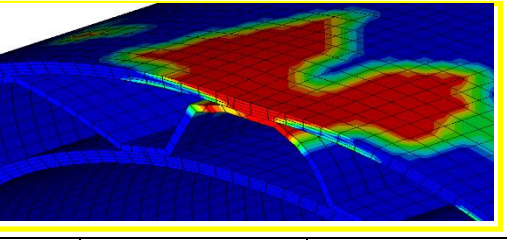
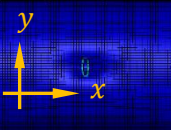
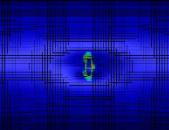
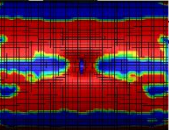
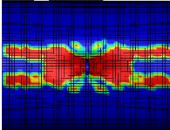
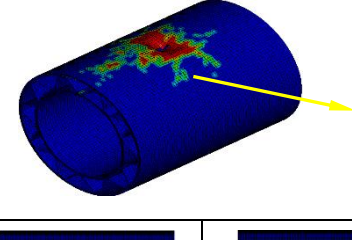
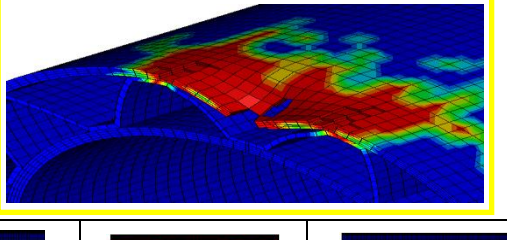
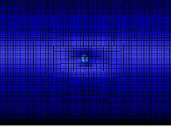
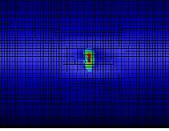
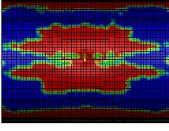
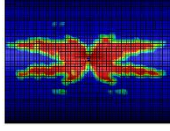


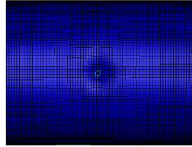
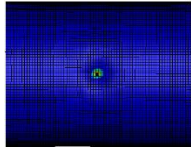
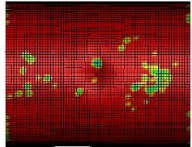
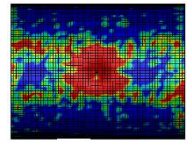
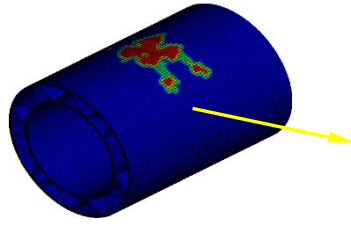
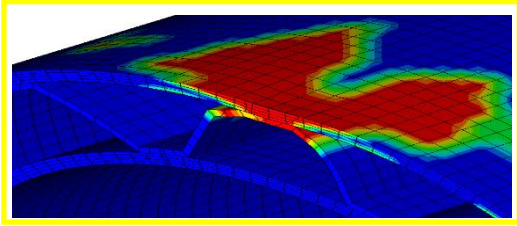
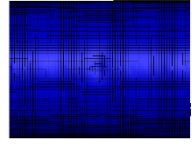
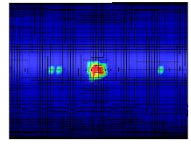
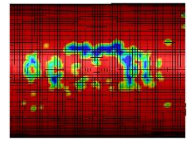
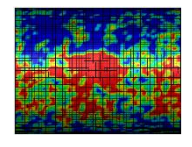
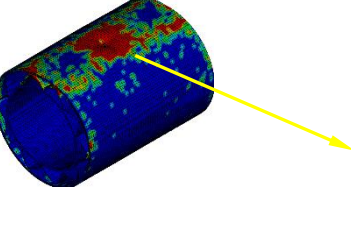
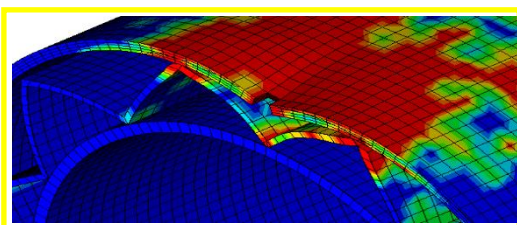
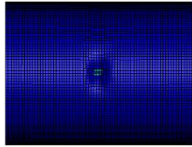
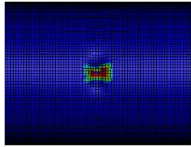
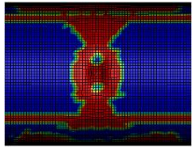
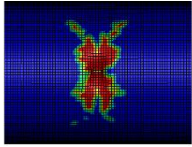
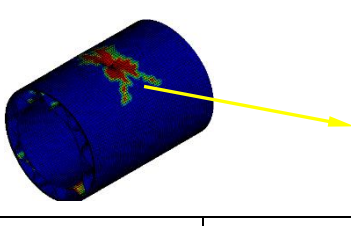
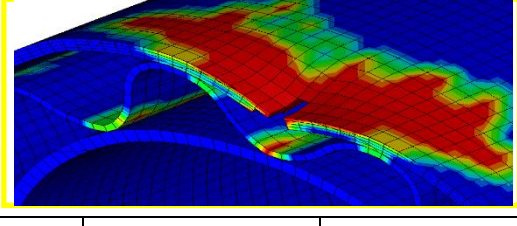
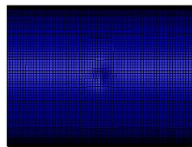
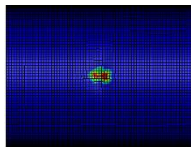
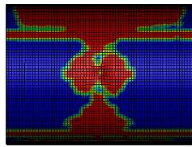
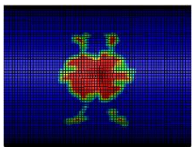
Figure 10. Deformations at critical points in trapezoidal sandwich structure.

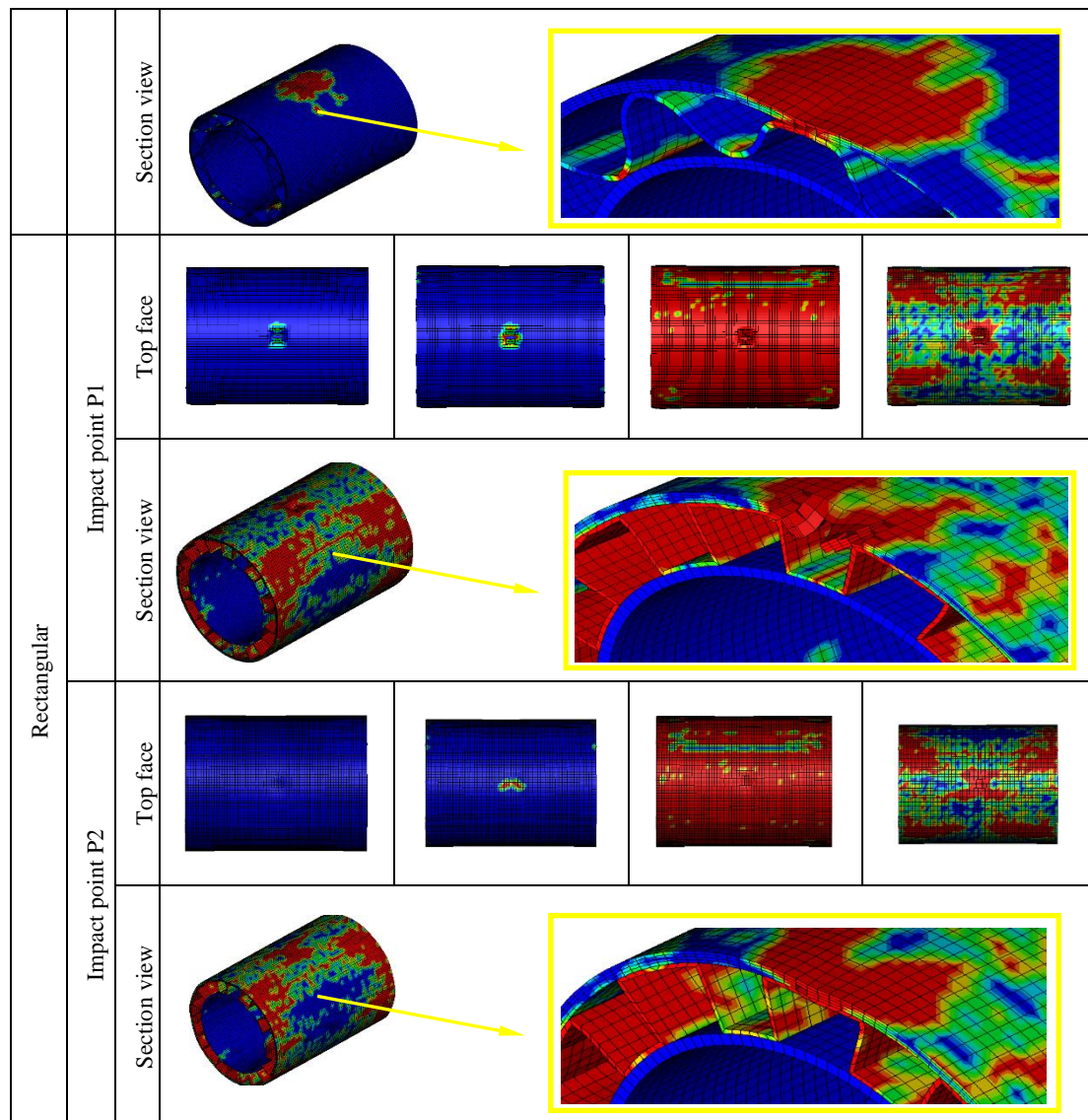
Table 6 shows the Tensile fiber mode, Compressive fiber mode, Tensile matrix mode and Compressive matrix mode damages of sandwich composite structures with different core structures. The damages for 10 J impact for five different core structures are compared. Here, the regions shown in red color represent the damaged areas and the regions shown in blue represent the areas where no damage occurred [21].

First of all, it is seen that the deformation at point P1 is large because it is not supported by the core [22]. However, it was determined that the effect of the damage spread over a wider area. It was mentioned in the previous section that this effect causes large fluctuations in the graphic structures. At P2, the damage was more stable and localized compared to P1 since it was supported by the core structure [23]. Tensile matrix mode damage area among the core structures was found to be the highest in the Triangular structure. It is understood that the core structure is a very important parameter against impact [14], [24], [25].

Table 6. Deformations in sandwich structures.

10 J		Tensile fiber mode	Compressive fiber mode	Tensile matrix mode	Compressive matrix mode
Trapezoidal	Impact point P1				
	Impact point P1				
	Impact point P2				
	Impact point P2				
Arc shaped	Impact point P1				
	Impact point P1				
	Impact point				

Triangular	Impact point P1	Top face				
		Section view				
	Impact point P2	Top face				
		Section view				
Sinusoidal	Impact point P1	Top face				
		Section view				
	Impact point	Top face				



4. CONCLUSIONS

In this study, the impact performances of CFRP composite cylinder sandwich structures with five different geometric configurations were numerically investigated and compared with each other. In the study, the impact performances and damage types of composite cylinder structures for different core configurations were determined by *LS DYNA* finite element method. Based on the data obtained at the end of the study, the results can be summarized as follows:

- The PF value at point P2 is higher than P1. The effect of core support on PF is quite significant.
- The energy absorption efficiency value at P1 point is higher than P2 point.
- The highest peak force value was obtained at impact point P2 in the Trapezoidal sandwich structure. The lowest value was obtained at P1 impact point in Triangular sandwich structure.
- Energy absorption efficiency was highest and lowest in Triangular with 78% and 38%.
- In general, the energy absorption efficiency value increased as the impact energy increased.
- Since it is not supported by the core at P1, the resulting deformation is larger than P2.
- When this numerical study is supported by an experimental study, it will have a high potential to contribute to the literature.

DECLARATION OF ETHICAL STANDARDS

The author declares that all ethical guidelines including authorship, citation, data reporting, and publishing original research are followed.

DECLARATION OF COMPETING INTEREST

The author declares that there is no conflict of interest.

FUNDING / ACKNOWLEDGEMENTS

This study did not receive funding from any provider.

5. REFERENCES

- [1] Y. Rong, J. Liu, W. Luo, and W. He, "Effects of geometric configurations of corrugated cores on the local impact and planar compression of sandwich panels," *Compos B Eng*, vol. 152, no. August, pp. 324–335, 2018, doi: 10.1016/j.compositesb.2018.08.130.
- [2] W. He, J. Liu, B. Tao, D. Xie, J. Liu, and M. Zhang, "Experimental and numerical research on the low velocity impact behavior of hybrid corrugated core sandwich structures," *Compos Struct*, vol. 158, pp. 30–43, 2016, doi: 10.1016/j.compstruct.2016.09.009.
- [3] X. Xue, C. Zhang, W. Chen, M. Wu, and J. Zhao, "Study on the impact resistance of honeycomb sandwich structures under low-velocity/heavy mass," *Compos Struct*, vol. 226, no. May, p. 111223, 2019, doi: 10.1016/j.compstruct.2019.111223.
- [4] A. Tarafdar *et al.*, "Quasi-static and low-velocity impact behavior of the bio-inspired hybrid Al/GFRP sandwich tube with hierarchical core: Experimental and numerical investigation," *Compos Struct*, vol. 276, p. 114567, Nov. 2021, doi: 10.1016/J.COMPSTRUCT.2021.114567.
- [5] W. Chen, F. Wan, F. Guan, X. Liu, Y. Yang, and C. Zhou, "The effect of seabed flexibility on the impact damage behavior of submarine sandwich pipes," *Applied Ocean Research*, vol. 142, p. 103838, Jan. 2024, doi: 10.1016/J.APOR.2023.103838.
- [6] D. K. Korupolu, P. R. Budarapu, V. R. Vusa, M. K. Pandit, and J. N. Reddy, "Impact analysis of hierarchical honeycomb core sandwich structures," *Compos Struct*, vol. 280, p. 114827, Jan. 2022, doi: 10.1016/J.COMPSTRUCT.2021.114827.
- [7] J. S. Yang *et al.*, "Low velocity impact behavior of carbon fibre composite curved corrugated sandwich shells," *Compos Struct*, vol. 238, no. August 2019, pp. 1–16, 2020, doi: 10.1016/j.compstruct.2020.112027.
- [8] I. Bozkurt, "Effect of geometric configurations and curvature angle of corrugated sandwich structures on impact behavior," *Polym Compos*, pp. 1–24, 2024.
- [9] A. İ. Ayten, "Investigation of mechanical properties and damage types of E-glass fiber reinforced epoxy matrix composites under various loadings," *International Advanced Researches and Engineering Journal*, vol. 7, no. 3, pp. 185–190, 2023, doi: 10.35860/iarej.1334883.
- [10] L. Gemi, M. Kara, and A. Avci, "Low velocity impact response of prestressed functionally graded hybrid pipes," *Compos B Eng*, vol. 106, pp. 154–163, Dec. 2016, doi: 10.1016/J.COMPOSITESB.2016.09.025.
- [11] L. Zheng, F. Q. Li, W. Da Wang, and Y. L. Shi, "Bionic corrugated sandwich cylindrical tubes subjected to transverse impact," *Structures*, vol. 64, p. 106599, Jun. 2024, doi: 10.1016/J.ISTRUC.2024.106599.

- [12] W. He, J. Liu, S. Wang, and D. Xie, "Low-velocity impact response and post-impact flexural behaviour of composite sandwich structures with corrugated cores," *Compos Struct*, vol. 189, no. January, pp. 37–53, 2018, doi: 10.1016/j.compstruct.2018.01.024.
- [13] W. He, J. Liu, S. Wang, and D. Xie, "Low-velocity impact behavior of X-Frame core sandwich structures – Experimental and numerical investigation," *Thin-Walled Structures*, vol. 131, no. July, pp. 718–735, 2018, doi: 10.1016/j.tws.2018.07.042.
- [14] I. Bozkurt, M. O. Kaman, and M. Albayrak, "Low-velocity impact behaviours of sandwiches manufactured from fully carbon fiber composite for different cell types and compression behaviours for different core types," *Materialpruefung/Materials Testing*, vol. 65, no. 9, pp. 1349–1372, 2023, doi: 10.1515/mt-2023-0024.
- [15] H. JO., *LS-DYNA Keyword User's Manual Volume II Material Models, Version 971. Livermore Software Technology Corporation; . [24]. 2017.*
- [16] L. Gemi, M. Kayrıci, M. Uludağ, D. S. Gemi, and Ö. S. Şahin, "Experimental and statistical analysis of low velocity impact response of filament wound composite pipes," *Compos B Eng*, vol. 149, pp. 38–48, Sep. 2018, doi: 10.1016/J.COMPOSITESB.2018.05.006.
- [17] F. Dogan, H. Hadavinia, T. Donchev, and P. S. Bhonge, "Delamination of impacted composite structures by cohesive zone interface elements and tiebreak contact," *Central European Journal of Engineering*, vol. 2, no. 4, pp. 612–626, 2012, doi: 10.2478/S13531-012-0018-0.
- [18] I. Bozkurt, M. O. Kaman, and M. Albayrak, "Experimental and numerical impact behavior of fully carbon fiber sandwiches for different core types," *Journal of the Brazilian Society of Mechanical Sciences and Engineering*, vol. 46, no. 5, p. 318, May 2024, doi: 10.1007/s40430-024-04865-3.
- [19] Z. Hashin, "Failure criteria for unidirectional fiber composites," *Journal of Applied Mechanics, Transactions ASME*, vol. 47, no. 2, pp. 329–334, 1980, doi: 10.1115/1.3153664.
- [20] M. Albayrak, M. O. Kaman, and I. Bozkurt, "Experimental and Numerical Investigation of the Geometrical Effect on Low Velocity Impact Behavior for Curved Composites with a Rubber Interlayer," *Applied Composite Materials*, vol. 30, no. 2, pp. 507–538, 2023, doi: 10.1007/s10443-022-10094-5.
- [21] B. A. Gama, T. A. Bogetti, and J. W. Gillespie Jr, "Progressive Damage Modeling of Plain-Weave Composites using LS-Dyna Composite Damage Model MAT162," *7th European LS-DYNA Conference*, no. August 2014, 2009.
- [22] A. M. Bozkurt İ, Kaman MO, "LS-DYNA MAT162 Finding Material Inputs and Investigation of Impact Damage in Carbon Composite Plates. XVI. international research conference 2022.," 2022.
- [23] J. Liu, W. He, D. Xie, and B. Tao, "The effect of impactor shape on the low-velocity impact behavior of hybrid corrugated core sandwich structures," *Compos B Eng*, vol. 111, pp. 315–331, 2017, doi: 10.1016/j.compositesb.2016.11.060.
- [24] T. Zhao *et al.*, "An experimental investigation on low-velocity impact response of a novel corrugated sandwiched composite structure," *Compos Struct*, vol. 252, no. June, p. 112676, 2020, doi: 10.1016/j.compstruct.2020.112676.
- [25] M. O. Kaman, M. Y. Solmaz, and K. Turan, "Experimental and numerical analysis of critical buckling load of honeycomb sandwich panels," *J Compos Mater*, vol. 44, no. 24, pp. 2819–2831, 2010, doi: 10.1177/0021998310371541.